Development and Benchmark calculations of Monte Carlo Transport Program MATS for R&D of Accelerator-Driven System*

Xiao-Qiang Wei,[1,2] Han-Jie Cai,[1,2,†] Xun-Chao Zhang,[1,2] Neng Pu,[1,2] Peng Fang,[1,2] Huan Jia,[1,2] Yuan He,[1,2,‡] Yong-Wei Yang,[1,2] Rong Wang,[1,2] Mingfei Yan,[3,4] Xiao-Chong Zhu,[1,2] Peng Hui,[1,2] and Xin-Yuan Luo[1,2]

[1]Institute of Modern Physics, Chinese Academy of Sciences, Lanzhou 730000, China
[2]School of Nuclear Science and Technology, University of the Chinese Academy of Sciences, Beijing 100049, China
[3]School of Energy and Power Engineering, Xi'an Jiaotong University, Xi'an 710049, China
[4]RIKEN Center for Advanced Photonics, RIKEN, Wako 351-0198, Japan

Accelerator-driven System (ADS) is widely regarded as the most effective transmutation solution of nuclear waste. The Monte Carlo transport simulation of full-energy-range particles, which are involved in both the spallation target and the sub-critical blanket, forms the foundation of ADS simulation studies. A Monte Carlo program named MATS has been developed in conjunction with the ADS research activities and development projects in China, with the aim of achieving key technology breakthroughs as well as facility construction. The development background of the program, the transport framework and functional modules developed for full-energy-range transport, the validations and the conclusions are introduced. The benchmark calculations of the OECD-ADS model show that MATS be used to perform ADS physical studies with reasonable deviations for both the spallation target and the sub-critical reactor.

Keywords: accelerator-driven system, Monte Carlo program, MATS1.0, code development, benchmark calculations

I. INTRODUCTION

The idea of sustaining fission reactions in a sub-critical reactor with external neutrons from a spallation target, known as the concept of the Accelerator-Driven Subcritical (ADS) system, was proposed in 1990s [1] as a potential technology for developing safe, sustainable and clean nuclear fission energy. From 1990s to 2010s, several conceptual designs of ADS ranging from hundreds to thousands of Megawatts were proposed, such as EFIT, ANL ADS and JAEA ADS [2–5]. As an intermediate step towards the industrial prototype of an ADS, the construction of an experimental facility is essential. Currently, the MYRRHA [6] and CiADS [7, 8] projects are under the active developments of experimental ADS devices.

To reduce technical risks and to suppress investment costs, the MYRRHA project has been planned [9] to begin with a 100 MeV accelerator, followed by the 100-600 MeV accelerator section [2] and finally the reactor [3]. The CiADS project is more ambitious. According to the CiADS project schedule, the construction of the facility, which includes a 500-MeV accelerator, a LBE (Lead-Bismuth Eutectic) target and a sub-critical reactor, is expected to be finished by 2027. The 500 MeV proton beam is anticipated to be achieved by 2025, with a current of 50 mA. The power ramping to 250 kW and 2.5 MW are expected to be achieved by 2027 and 2029, respectively.

An ADS is a combination of a high-power accelerator, a spallation target and a sub-critical fission blanket. Research and Development (R&D) of the sub-critical system demands simulation toolkit not only for the fission blanket but also for the spallation target. Simulation of particles across a broad energy spectrum, from eV or keV up to GeV, are necessary to analyze the physical parameters. Given the complexity of reactions induced by energetic particles in the spallation energy range and the scarcity of experimental data, the transport of the particles above several hundred MeV primarily relies on intra-nuclear cascade and de-excitation models. In general, the simulation of ADS can be divided into two steps: (1) simulating the beam-target interaction process and the transport of secondary protons and neutrons to obtain the details of the external neutron source and (2) simulating the reactor with the external neutron source [10]. In the first step, general-purpose particle transport programs such as Geant4 [11], FLUKA [12], MARS [13] and PHITS [14], or specialized programs like EA-MC [15], HERMES [16], HETC [17], NMTC [18] and LAHET [19], can be utilized. In the second step, deterministic neutron transport programs are preferred in earlier years due to their computational efficiency. For example, the ADS3D developed by JAEA [20] uses the general-purpose particle and heavy ion transport Monte Carlo program PHITS for the first-step simulation and employs the deterministic neutron transport program PARTISN [21] for the fixed-source calculation with the external neutron source data given by PHITS. The leaking neutrons below 20 MeV are stored and converted to the format for PARTISN by the FSOURCE module developed for the ATRAS code system [3] in the OMEGA

* Supported by the National Development and Reform Commission of China (Large Research Infrastructures of 12th Five-Year Plan: China initiative Accelerator Driven System, No. 2017-000052-75-01-000590) and the National Natural Science Foundation of China (No. 12475304)

† Corresponding author, 18693108957, caihj@impcas.ac.cn
‡ Corresponding author, hey@impcas.ac.cn

project.

The deterministic codes have always been the main tools for reactor physics analysis [22–25]. With the advancement of computing power, the number of Monte Carlo programs in nuclear reactor research and development has increased sustainably. Typical Monte Carlo programs such as MC21 [26], Serpent [27], JMCT [28], RMC [29, 30], SuperMC [31], NECP-MCX [32] and OpenMC [33] can be used for simulating the transport and reactions of low-energy neutrons in an ADS reactor. Compared to deterministic neutron transport program, Monte Carlo programs can provide more accurate and locally dependent neutronics characteristics in realistic 3D geometries of any complexity. Like the deterministic programs, when used in ADS simulation, the aforementioned Monte Carlo programs rely on external neutron information provided by the first-step simulation.

In the sub-critical reactor of ADS, a certain proportion of neutrons exceeds 20 MeV. Although relatively small in proportion, these high-energy neutrons play a pivotal role in defining the neutronics characteristics of the system. The Monte Carlo programs mentioned earlier are critical-reactor-oriented and based on nuclear data. The completeness and accuracy of nuclear data, particularly the scarcity of experimental data involving high-energy neutron interactions with Actinides, impose the limitations on the data-driven Monte Carlo programs in ADS simulations. At LANL, the program MCNPX [34] and its enhanced version of MCNP6 [35] have been developed to perform both reactor calculations and full-energy-range Monte Carlo simulations of ADS. MCNPX/MCNP6 integrates several functional modules and physical models, enabling the simulation of transport and reactions of high-energy particles in both the spallation target and the sub-critical blanket. This capability is essential, as the two-step methods tend to underestimate neutron fluence in the sub-critical reactor, resulting in an overestimation of beam requirement by 20% ∼ 30% [20]. Along with the development of the ADS facilities in China, a Monte Carlo program named MATS has been developed, enabling users to simulate the transport processes of proton, neutron, pion and main light nuclei in the full-energy range of ADS target-reactor system.

MATS is based on the GMT program [36, 37], which was developed by Institute of Modern Physics, CAS, for the simulation of ADS targets. It also incorporates the elements from OpenMC, an open-source reactor-oriented program developed by MIT. MATS implements the transport and physical codes from GMT in the framework of OpenMC. This enables a comprehensive simulation of the transport processes in an ADS, from the high-energy protons hitting the target to the neutronics characteristics in the sub-critical blanket.

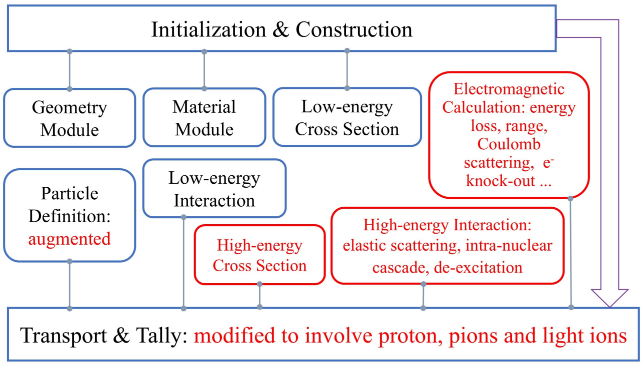

Fig. 1. (Color online) The modules and framework of MATS.

II. FRAMEWORK AND FUNCTIONAL MODULES DEVELOPED FOR FULL-ENERGY-RANGE TRANSPORT

A. Bases and framework of MATS

The Monte Carlo programs GMT and OpenMC each have distinct features dedicated for the transport simulations of high-energy charged particles and neutrons, respectively. OpenMC features the comprehensive modules for reactor calculation and tally functions [38]. MATS integrates the two programs by incorporating GMT's functional modules for charged particles and high-energy neutrons, including the electromagnetic calculation module, hadronic interaction simulation module, and high-energy cross-section module [36], into OpenMC's framework. As depicted in Fig. 1, the newly integrated modules for MATS are highlighted in red. Furthermore, the particle definition module, particle advance function and tally module have been extended, as illustrated in Fig. 2.

The basic particle definitions in OpenMC have been extended to include the particles necessary for ADS computations, such as proton, high-energy neutron (>20 MeV), pion and light nuclei from deuteron to carbon. In the initialization stage of the program, MATS incorporates the ionization energy loss calculation module from GMT. This process involves the establishment of energy loss-range relationship for each charged particle (excluding the general ions) and each nuclide, and storing the data in memory as a hash table for direct retrieval during the subsequent particle transport process.

Once the cross-section calculations are completed, the particles proceed to move forward. Since the advance processes of charged particles are significantly different from that of neutrons, MATS adopts the charged particle transport method from GMT. Charged particles are advanced step by step using the same ray-tracing technique as GMT, until a collision event happens. The loop terminates only when the particle reaches a collision point or when its energy falls below the low-energy cutoff. If a particle survives after a track without interaction, it

will traverse the current geometric entity. Before that, the particle is positioned at the surface of the next geometric entity. In this scenario, the particle has reached the boundary, so its spatial position remains unchanged; only the geometric entity it is associated with is updated.

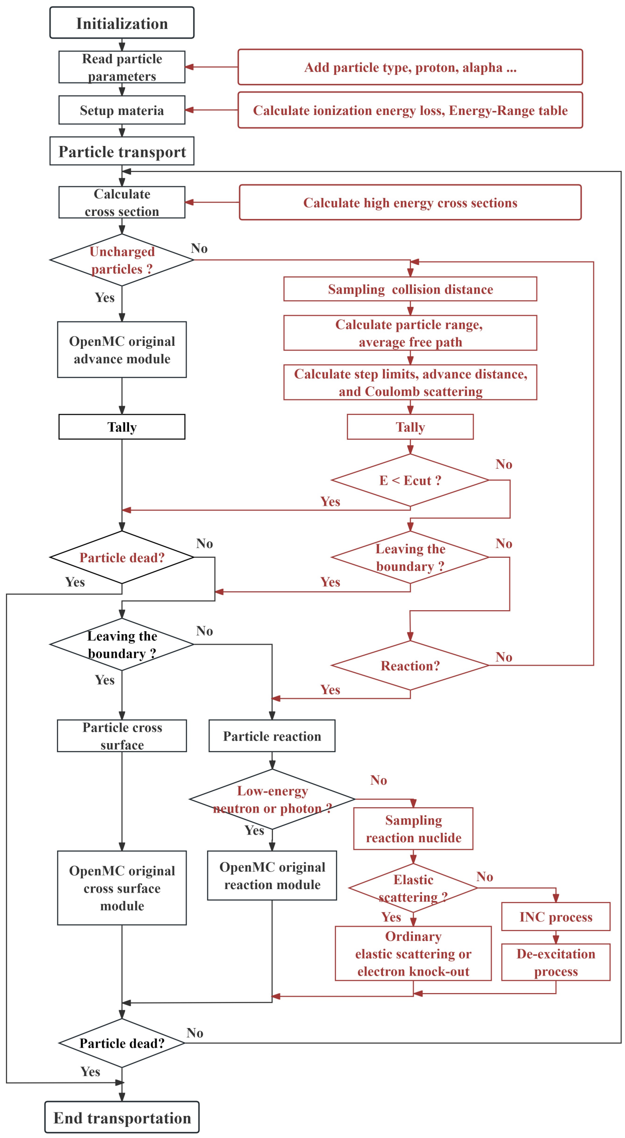

Fig. 2. (Color online) The entire flow chart of MATS program.

When a particle reaches a collision position, for neutron, photon with energies below 20 MeV, MATS employs the original processing code from OpenMC. For particles in other scenarios, the hadronic interaction module is utilized. In the case of ordinary elastic scattering, the program directly computes the scattering angle, with the particle changing direction and losing energy accordingly. In the case of electron knock-out scattering, the program first calculates the energy of the knocked-out electron and samples its direction. Then it calculates the scattering angle for the incident particle. Ultimately, this process results in the production of an electron, with the energy and direction of the incident particle being altered.

In MATS, the original post-processing functions of OpenMC have been modified to accommodate new transport and reaction modules. This includes statistical analysis of heat production, flux, reaction rates of high-energy interactions, and time-dependent phenomena. As depicted in Fig. 2, via the combination of the functions of the two programs, MATS has gained the capability to simulate the entire physical process, from proton-target interactions to the subsequent transport of secondary particles in both the spallation target and the sub-critical blanket. This is particularly relevant in the simulation of an ADS subcritical system.

B. High-energy cross section module

OpenMC is typically capable of calculating reaction cross-sections for neutron, photon at energies below 20 MeV, depending on the nuclide cross-section database used. In cases where the energy of a neutron is above 20 MeV or when dealing with new particles, MATS directly derives the high-energy cross-sections for elastic scattering, inelastic scattering, and electron knock-out process, utilizing the cross-section module from GMT.

Within MATS, the Glauber calculation method [39] in combination with a data-based approach is employed to calculate the strong interaction cross-section. This includes the calculations of both elastic and non-elastic reaction cross-sections between hadrons and atomic nuclei, as well as between nuclei themselves. For proton and pion elastic and non-elastic reactions with atomic nuclei, where there is a wealth of experimental or evaluated data (representative elements such as aluminum, copper, and lead), the cross-section data are listed and stored. When calculating proton and pion reaction cross-sections, empirical fitting and interpolation based on the listed data can be applied to obtain better accuracy.

C. Electromagnetic and tracking modules

The electromagnetic module of the program calculates the ionization/excitation energy loss based on the Bethe-Bolch formula, as shown in Eq. (1).

$$-\frac{dE}{dx} = 4\pi N_A r_e^2 m_e c^2 z^2 \frac{Z}{A}\frac{1}{\beta^2} \times \left(\frac{1}{2}\ln\frac{2m_e c^2\beta^2\gamma^2 T_{\max}}{I^2} - \beta^2 - \frac{\delta}{2}\right) \quad (1)$$

In the equation, z represents the charge of the incident particle; Z and A denote the atomic number and the mass number of the material's atoms, respectively; m_e

stands for the charge of an electron; r_e signifies the classical electron radius; N_A denotes Avogadro's constant; I represents the average excitation energy; and δ signifies the density effect correction.

During the initialization of the program, the energy deposition rate dE/dx is precalculated for the materials specified in the model, thereby determining the ranges of charged particles at various energies in different materials. This computed data is then stored in the tabular format for efficient and direct retrievals during subsequent particle transport simulations.

In electromagnetic process of Coulomb scattering, the program employs the multiple scattering method, which is grounded in the Molière theory. This method is used for the distribution of Coulomb scattering angles [40], and is applicable to the charged particles in wide energy range.

For charged particles, the electromagnetic process is continuous, making it impossible to calculate the collision distance directly as done in neutron transport. Our program uses the ray-tracking method to determine the physical collision points of charged particles. This method is combined with the step limits of the particles to determine their transporting distances.

This method uses the concept of n_λ in particle transport process, converting the collision distance into a specific coefficient of the mean free path:

$$n_\lambda = \int_{x_1}^{x_2} \frac{dx}{\lambda(x)} \tag{2}$$

The randomized value n_λ follows the following probability distribution:

$$P(n_r < n_\lambda) = 1 - e^{-n_\lambda} \tag{3}$$

Therefore, the sampling formula for n_λ is derived as follows:

$$n_\lambda = -\log(\eta) \tag{4}$$

where η represents a random variable uniformly distributed in the interval (0, 1). Once n_λ is determined through sampling, it is then updated at each step of the particle's track, which is expressed as:

$$n'_\lambda = n_\lambda - \frac{\Delta \mathrm{x}}{\lambda(\mathrm{x})} \tag{5}$$

When n'_λ is sufficiently small, it indicates that the particle has reached the collision point to collide, thus ending its current advancement.

D. Hadronic interaction modules

In the process of hadronic interaction during particle transport, the most crucial aspect is the spallation reactions of high-energy particles. Spallation is one type nuclear reaction where a relativistic hadron or light nucleus bombard a high mass number nucleus, triggering a cascade of intranuclear hadronic interactions and deexcitation processes. This reaction results in the emission of a large number of hadrons (primarily neutrons, protons, and pions) and light-nucleus particles. Typically, the de-excitation process is accompanied by the production of fission fragments.

As previously mentioned, the spallation reaction can generally be divided into two stages: the Intra-Nuclear Cascade (INC) process and the de-excitation process of residual nucleus [41, 42]. Several INC models and evaporation/fission models have been developed over the past three decades. INC models, such as CEM, BERTINI, ISABEL, and INCL, have been widely adopted in Monte Carlo programs. In the domain of evaporation/fission models, the eminent contenders such as ABLA [43] and DRENSER [44] manifest. Beyond the INC and deexcitation processes, it is generally accepted that a pre-equilibrium process exists between the two processes. This process allows the highly excited residual nucleus transits to an equilibrium compound nucleus by emitting a neutron or a light charged particle with slightly higher energy than those evaporated during the deexcitation process. In many Monte Carlo programs, the pre-equilibrium process is often not explicitly considered, mainly because many INC models have already implemented it.

The reliability of using the INCL model to simulate particle-nucleus interactions within the GMT framework has been meticulously substantiated [36], along with the ABLA [43] model for heavy residual nucleus deexcitation and the Fermi Break-up model for the light ones. MATS has integrated these three models, making them more modular and easily disabled or replaced with minor modifications, thus facilitating subsequent program updates. For elastic interaction, MATS employs the well-established Glauber model, effectively simulating the elastic nuclear scattering process. It is noteworthy that the electron knock-out process mentioned in the electromagnetic module is also classified as one type of elastic interaction in the program.

III. BENCHMARK CALCULATIONS

A. The benchmark model

The OECD-ADS model, a 377 MWth small-size ADS sub-critical blanket, is chosen for the numerical validations of MATS. Proposed by the Organization for Economic Cooperation and Development/Nuclear Energy Agency (OECD/NEA) in collaboration with seven institutions(ANL, CIEMAT, KAERI, JAERI, PSI/CEA, RIT and SCK•CEN), this benchmark model is designed to compare the ADS neutronics parameters utilizing various programs and Evaluated Nuclear Data Libraries [45]. In the benchmark calculations, a predefined

spallation neutron source produced with HETC was provided assuming a proton energy of 1 GeV and a beam radius of 10 cm, was provided to the participants for reactor calculations applying both deterministic and Monte Carlo codes.

Fig. 3 shows the OECD-ADS benchmark model. The concept includes four fuel regions. The central region represents the target area, with the void region above it housing the beam pipe space. Encircling the target area is the fuel region, and the outermost layer is the reflector region. Details of the materials in the target, fuel, and reflector regions of the model can be found in the reference for the OECD/NEA benchmark work [45].

A cylindrical target made of lead-bismuth eutectic (LBE) material was modeled, with a height of 150 cm and a radius of 20 cm. The Cartesian coordinate system was adopted, with the origin set at the center of the target's bottom surface, and the cylinder axis defined as the Z-axis. Surrounding the target, a fuel region was modeled with a height of 100 cm, an inner radius of 20 cm and an outer radius of 92 cm. A cylindrical reflector region with a thickness of 50 cm was constructed to encompass the fuel region. An ideal beam of uniformly distributed protons with a radius of 10 cm was directed towards the target at the coordinates (0, 0, 150) with a direction vector of (0, 0, -1). In the simulation, the ENDF/B-VII.0 database was used for neutron calculation, while the photon data was obtained from the ENDF/B-VII.1 database.

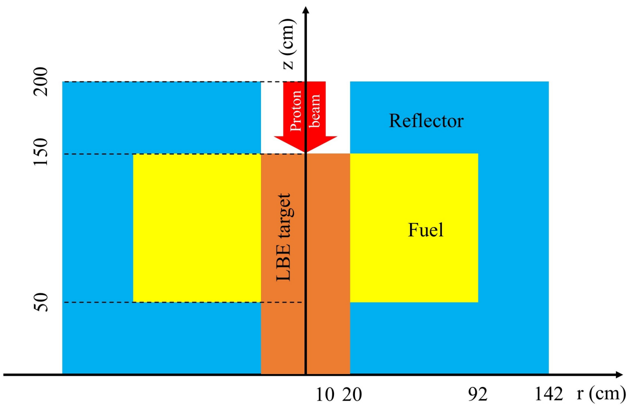

Fig. 3. (Color online) The OECD-ADS benchmark model.

B. Benchmark calculations of spallation target

1. Neutron fluence and neutron yield

The physical processes within the target, including electromagnetic and hadronic interactions, directly determine the yield and energy spectrum of leakage neutrons, both of which are crucial for the computation of sub-critical reactor system. The simulation was carried out with 1 million proton particles, each with an energy of 1 GeV, directed towards the target as described in previous subsection. The resulting neutron fluence distribution, heat deposition distribution within the target, and leakage neutron energy spectrum were obtained. The results from MATS were compared with those from other Monte Carlo programs, including MCNPX 2.5.0, Geant4, and PHITS. For both MATS and Geant4 simulations, the INC model used was INCL++ [46], with MATS employing version 5.1 and Geant4 employing version 6.28. To minimize discrepancies caused by different physical models, the INCL model was also selected for PHITS and MCNPX simulations. PHITS used INCL4.6 [47], while MCNPX used INCL4.2. Both programs are in Fortran. It is worth noting that INCL4.6 is the last Fortran version of INCL model and after that it was only distributed in C++.

Fig. 4 illustrates the axial (H) and radial (R) distributions of neutron fluence within the target, calculated by different programs. Meanwhile, Fig. 5 displays the two-dimensional spatial distributions in H and R directions. The axial and radial distributions of neutron fluence exhibit discernible differences among different programs. As demonstrated in the figures, MATS agrees more with Geant4 and PHITS, yet gives a lower estimation than MCNPX. This may be attributed to the fact that MATS has adopted the newer version of INCL model, similar to Geant4 and PHITS. INCL++ is based on INCL4.6 and has evolved significantly since it has been completely redesigned and rewritten in C++ in 2012. The difference between MATS and MCNPX is about 10%. As depicted in Fig. 5(a-d), the spatial distribution of neutron fluence within the target computed by MATS is roughly the same as those obtained by other programs. Fig. 5(e-g) illustrate the differences of the spatial distributions of neutron fluence between MATS and other programs (MCNPX, PHITS and Geant4). It is evident that MATS has the smallest discrepancy with Geant4.

Disparities in neutron fluence within the target can lead to variations in the yield and distribution of leaked neutrons, resulting in different beam requirements for the ADS subcritical system. In addition to the flux, the energy spectrum of leaked neutrons from the target also has a significant impact on the neutronics performance of the ADS sub-critical blanket. The normalized spectra of leaked neutrons calculated with MATS, MCNPX, Geant4 and PHITS programs are presented in Fig. 6. For neutrons with energies greater than 0.1 MeV - fast neutrons and high-energy neutrons that are absolutely dominant - the differences among the four programs are relatively indistinguishable. As detailed in table 1, MATS agrees very well with Geant4 in the range of 1 MeV to 20 MeV, while generally provides a lower prediction than MCNPX. Compared with PHITS, MATS tends to underestimate the yield of high-energy neutrons by less than 5% and overestimate the number of neutrons below 20 MeV by a similar margin. Regarding the total neutron yield, the difference between MATS and Geant4 is less

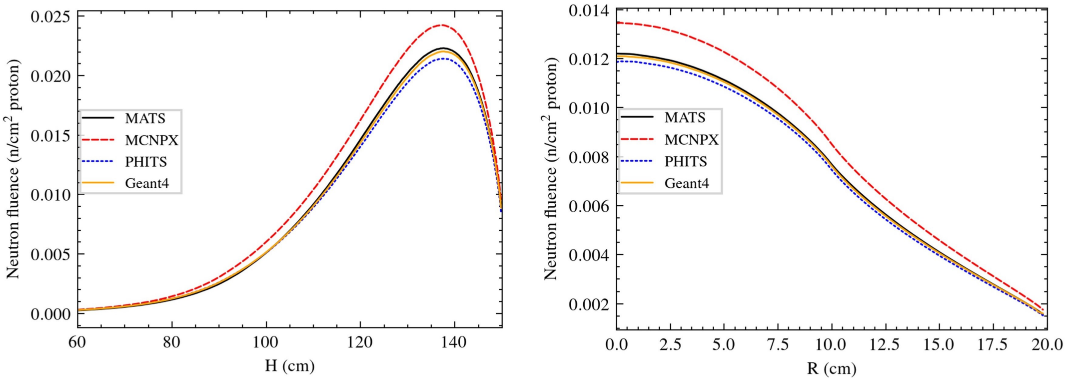

Fig. 4. (Color online) Comparisons of axial (left) and radial (right) distributions of neutron fluence in the target from the calculations of different Monte Carlo programs.

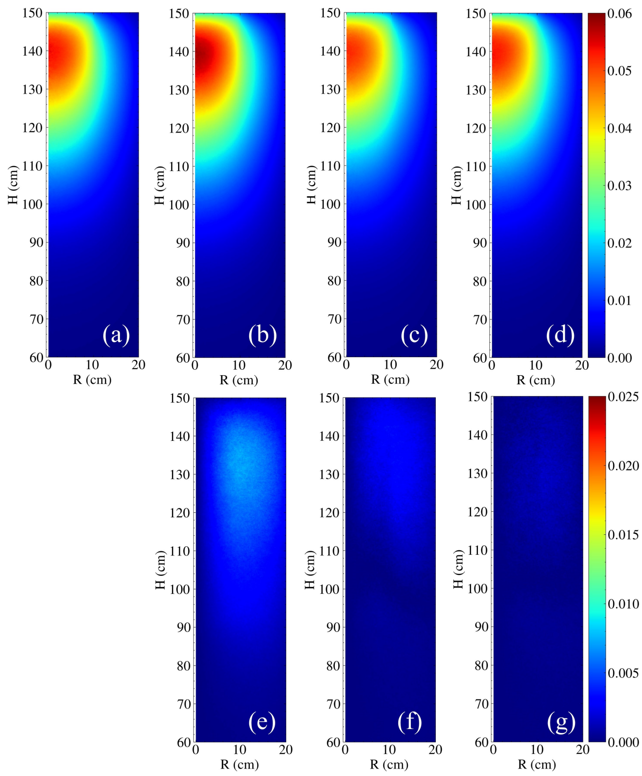

Fig. 5. (Color online) Neutron fluence (1/cm^2/proton) distributions evaluated with MATS (a), MCNPX (b), PHITS (c), Geant4 (d), and the deviations of other programs' results (MCNPX (e), PHITS (f), Geant4 (g)) compared to that of MATS.

than 1%, while the difference between MATS and MCNPX is about 10%.

2. Energy deposition in spallation target

The calculation of energy deposition in the target is crucial for the design of a spallation target. Fig. 7 shows

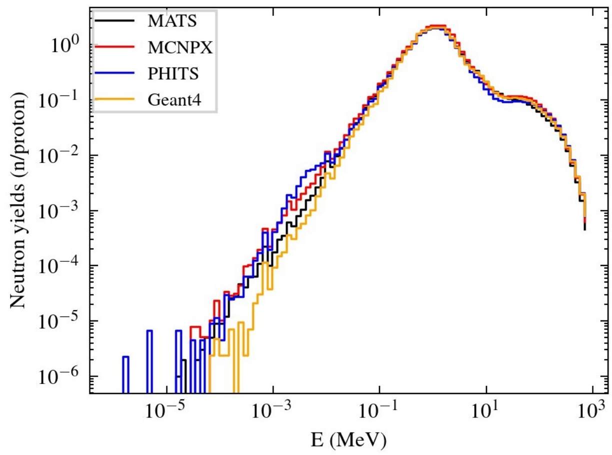

Fig. 6. (Color online) Normalized spectra of leaking neutron calculated by different programs.

the R-Z distributions of energy deposition simulated with MATS (a), MCNPX (b), PHITS (c), Geant4 (d), and the absolute deviations of other programs (MCNPX (e), PHITS (f), Geant4 (g)) compared to MATS, in unit of MeV/cm^3/proton. It is evident that the heat distributions within the target calculated by different programs are generally similar, except that MCNPX gives an overall underestimation, while MATS provides a slightly lower profile at the end of the range. The total energy deposition and its relative deviation are detailed in table 2, in unit of MeV/proton. MATS's result is about 3% higher than PHITS's result, and is nearly equivalent to Geant4's result. Interestingly, MCNPX underestimates the energy deposition while overestimates the neutron yield, with the magnitude of underestimation in energy deposition being nearly equivalent to the overestimation in neutron yield. This can be easily understood with energy conservation, since the overestimated neutrons take away more energy.

TABLE 1. Number of leaking neutrons from spallation target in different energy range evaluated with MATS, MCNPX, PHITS and Geant4 simulations.

Simulation	n/p				Difference (%)			
Programs	>20 MeV	1-20 MeV	<1 MeV	SUM	>20 MeV	1-20 MeV	<1 MeV	SUM
MATS	0.929	12.71	10.07	23.71	/	/	/	/
MCNPX	1.115	14.02	10.53	25.67	20.05	10.33	4.57	8.27
PHITS	0.968	12.02	9.71	22.70	4.20	-5.44	-3.55	-4.26
Geant4	1.033	12.81	9.73	23.57	11.27	0.78	-3.41	-0.59

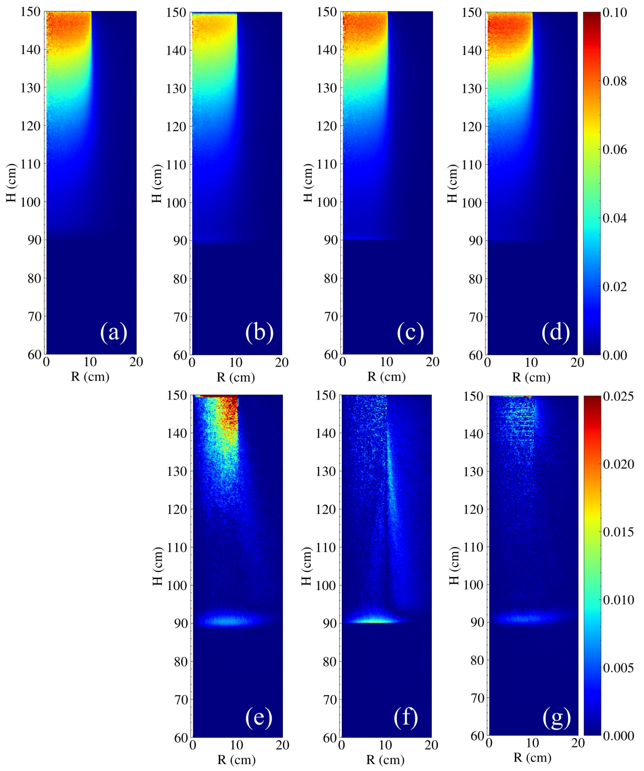

Fig. 7. (Color online) Similar to Fig. 5, but with the data energy deposition (MeV/cm^3/proton)

TABLE 2. Total energy deposition by 1 GeV proton on a LBE target simulated with different programs.

	Total heating (%)	
Programs	value (MeV/p)	Difference (%)
MATS	675.0	/
MCNPX	609.6	-9.69
PHITS	652.9	-3.27
Geant4	694.9	2.95

C. Benchmark calculations of target-reactor system

1. External source efficiency

In R&D of ADS, the external source efficiency φ^* serves as a crucial parameter for assessing the performance of the system [48]. It plays a pivotal role in determining the beam requirements, and its value can be evaluated by Monte Carlo simulation [10]. The φ^* is calculated with the following formula:

$$\varphi^* = \frac{1 - 1/k_{eff}}{1 - 1/k_s} \tag{6}$$

$$k_s = \frac{R\bar{v}}{(R\bar{v} + S_0)} \tag{7}$$

where k_s is the external source multiplication factor, R denotes the fission rate in the sub-critical blanket, $\bar{v}$ is the average number of neutrons released per fission, and S_0 is the intensity of the external neutron source. Normalizing each value to one external source neutron, the following equation is obtained:

$$\varphi^* = \frac{R\bar{v}}{S_0}\left(\frac{1}{k_{eff}} - 1\right) \tag{8}$$

showing φ^* as equivalent neutrons induced by an external source. A larger φ^* means a smaller ratio of absorption loss to fission yield. The external source efficiencies obtained with MCNPX and MATS are compared in Fig. 8. One sees that the higher the energy, the larger the external neutron efficiency. Furthermore, the efficiency tends to increase exponentially with $\log(E)$ above 10 MeV. Within the energy range of 0.01 MeV to 1000 MeV, MCNPX and MATS basically agree with each other. MATS exhibits a deviation of around 4% relative to MCNPX in the energy range of 100 MeV to 1000 MeV.

2. Notable contributions from high-energy neutrons

The conventional two-step simulations using reactor-oriented programs like OpenMC, often neglect high-energy neutrons in the calculation of sub-critical blanket due to database limitations. To mitigate this error, one approach is to reset the energy of high-energy neutrons to a value within the energy range of the database. However, the external source efficiency of high-energy neutrons is significantly higher than that of low-energy neutrons. To discuss the impact of neglecting high-energy neutrons in the sub-critical blanket, we consider the scenario where high-energy neutrons entering the fuel region from the target surface are reset to 20 MeV.

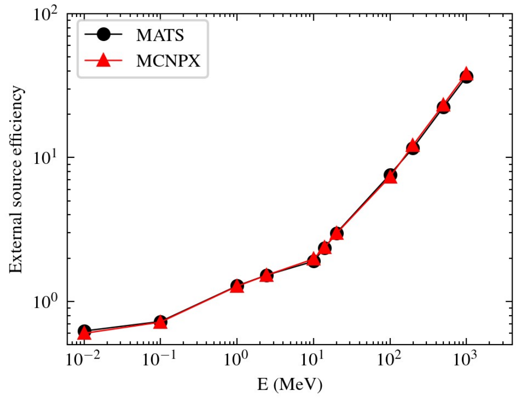

Fig. 8. (Color online) The external source efficiencies evaluated by MATS and MCNPX as a function of proton beam energy.

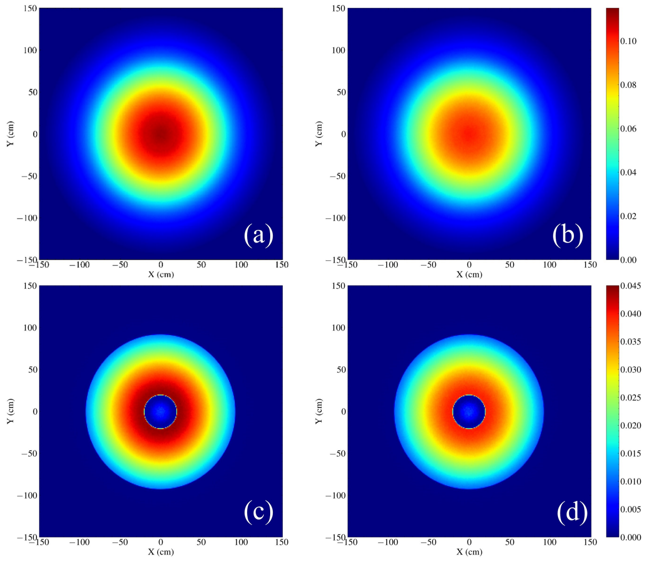

Fig. 9. (Color online) Comparisons in neutron fluence (n/cm^2/proton) and heat density (MeV/cm^3/proton) distributions between the complete transport scenario and the neutron-energy-cut transport scenario. (a) and (b) are for neutron fluence distributions, while (c) and (d) are for heat density distributions. (a) and (c) present the results under the complete transport scenario, while (b) and (d) present the results from the simulation without high-energy neutrons in fuel region. The profile distributions are present at the half-height (z = 100 cm) of the fuel.

Fig. 9(a) and 9(b) show the distributions of neutron fluence in the x vs.y plane at z=100 cm, with and without high-energy neutrons in fuel region, respectively. The differences are evident. The energy cutoff of neutrons results in an overall underestimation of neutron fluence. Fig. 10(a) presents the neutron fluence along x-axis at z = 100 cm and y = 0 cm, showing a relative deviation of approximately 10%. As previously mentioned, the larger the energy of a neutron, the higher its external source efficiency. Since the neutron fluence in the target region is partly contributed by neutrons form the fuel, the energy cutoff not only leads to an underestimation of neutron fluence in the fuel region, but also results in a reduced fluence within the target.

As shown in Fig. 9(c), 9(d) and 10(b), the heat density is nearly identical within the target region where the proton beam plays the dominant role for energy deposition. The deviation in the fuel region is similar to that observed for neutron fluence. An underestimation of neutron fluence will lead to an overestimation of the beam requirement [49]. The beam requirement represents the proton beam current needed to drive the reactor to operate at a fixed total power, which is expressed as:

$$I_p = \frac{W_R}{Q} \tag{9}$$

where W_R is the thermal power of the sub-critical blanket, and Q denotes the average heat released in the sub-critical blanket per proton.

With a total thermal power of 377 MW, the heat released in the sub-critical blanket are 55.9 GeV/proton per proton and 49.8 GeV/proton for complete transport and energy-cut transport simulations, respectively, as detailed in table 3. Consequently, the energy-cut transport simulation overestimates the beam requirement by more than 12%. In conclusion, the energy-cut transport method leads to significant deviations of design parameters. The capability to perform a complete transport simulation of the wide-energy-range particles in the sub-critical system is important not only for the design of an ADS, but also for in-core measurements and operational controls.

3. Cross validations

So far, only MCNPX and MCNP6 can be used for direct validations of MATS. To perform a comprehensive V&V, two-step methods have been employed, in addition to MCNPX. These methods involve using the neutrons leaking from the outer surface of a naked target, obtained from the first-step simulation, as an external source for the target-reactor in the second step. In all the two-step simulations, the neutrons in full-energy-range are transported.

Fig. 11 and 12 present the comparisons of neutron fluence and energy deposition distribution between the direct simulation and the two-step simulation. In the two-step simulation, denoted as MATS-MATS, full-energy-range external neutrons are transported in the sub-critical blanket, while other external particles are neglected. Fig. 11(a) shows the radial neutron distribution at z = 100 cm, while Fig. 11(b-d) display the axial neutron distributions at R = 0 cm, R = 22 cm and R = 56

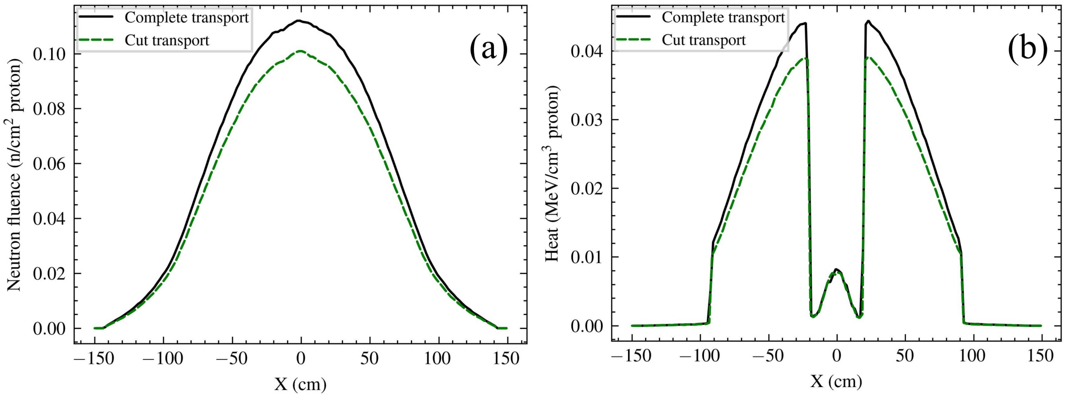

Fig. 10. (Color online) Neutron fluence distributions (a) and energy deposition distributions (b) along the x axis under the complete transport scenario and the energy-cut transport scenario at z=100 cm and y=0 cm in the target-reactor system.

TABLE 3. Heat released in the cub-critical blanket driven by one proton and the corresponding beam requirements.

Simulation methods	Heat released (GeV/p)	Beam requirements	
		Value (mA)	relative error (%)
Complete transport	55.9	6.744	/
Cut transport	49.8	7.569	12.22

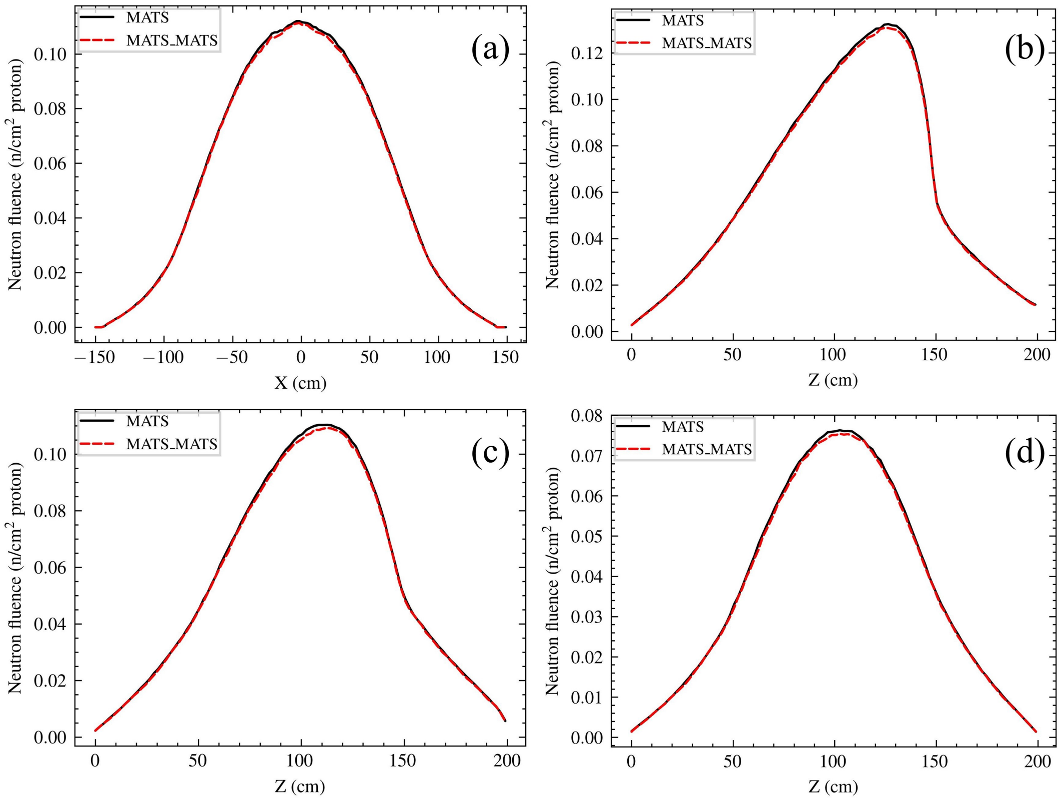

Fig. 11. (Color online) Neutron fluence distributions of the direct and two-step simulations using MATS. In the two-step simulation referred to as MATS-MATS, full-energy-range external neutrons are transported to the sub-critical blanket, while other external particles are disregarded. (a) is for radial neutron distribution at z = 100 cm. (b)(c)(d) are for axial neutron distributions at R = 0 cm, R = 22 cm and R = 56 cm, respectively.

cm, respectively. As shown in Fig. 11 and 12, the deviation in neutron fluence is at the level of 1%, while that in

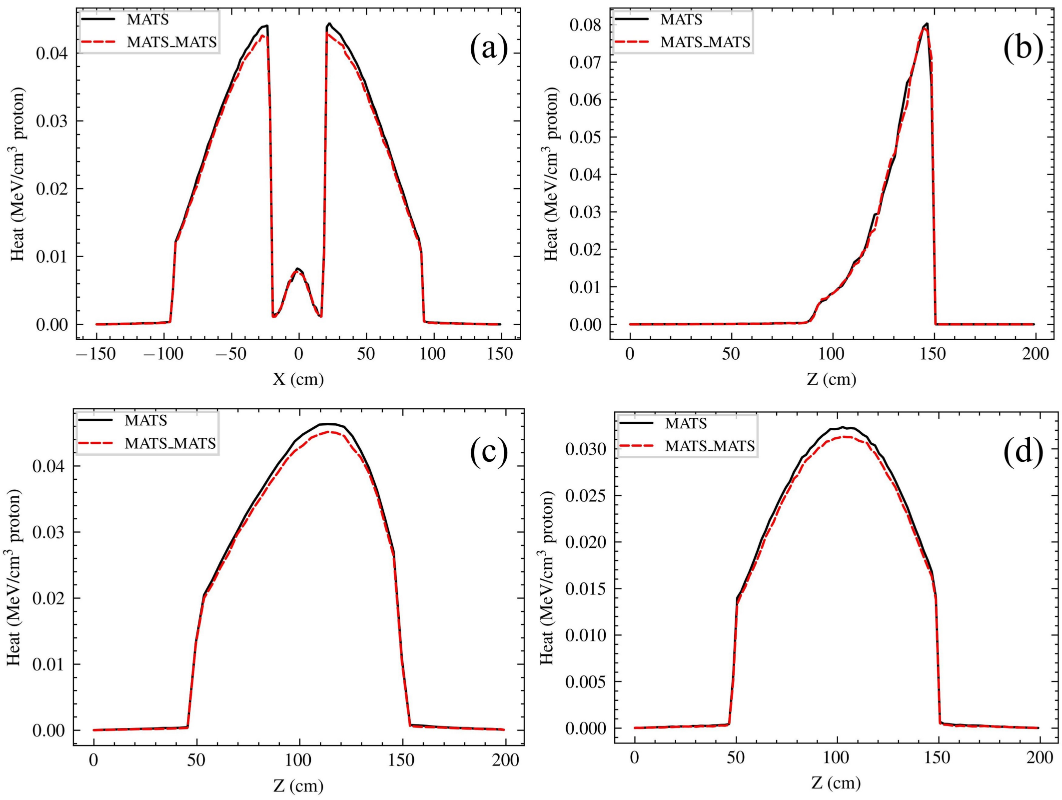

Fig. 12. (Color online) Similar to Fig. 11, but with the data representing heat density.

heat density is about 2%. These deviations can be eliminated when other external particles, including protons, pions, gammas and light-nucleus particles, are considered in the second-step simulation. Since these deviations are smaller than those caused by the differences of external neutrons from different programs, as previously described, the external particles other than neutrons are neglected in the two-step simulations to simplify the validation process, which will be detailed in the following section.

In Fig. 13 and 14, the direct MATS simulation is compared with the direct MCNPX simulation, and the two-step simulations that employ MCNPX, PHITS and Grant4 for the first-step simulation of neutron source. Since the second-step program is MATS, the conducted two-step simulations are denoted as MCNPX-MATS, PHITS-MATS and Grant4-MATS, respectively. For the radial distributions in Fig. 13(a) and 14(a), the target region ranges from -20 cm to 20 cm along the X-axis, while the fuel region ranges from -92 cm to 92 cm. The axial distributions in Fig. 13(b-d) and 14(b-d) display the results at three typical radial distances to the central axis. Fig. 13(b) and 14(b) are for the distributions in the beam-target region and Fig. 13(c-d) and 14(c-d) are for the distributions in the fuel region.

Clearly, one sees that the neutron fluences in both the target and fuel regions, as well as the heat density in the fuel region, are significantly higher from MCNPX and MCNPX-MATS simulations than that from MATS, PHITS-MATS and Geant4-MATS simulations. This finding is consistent with the results of neutron fluence and yield in the naked target simulation, as previously detailed. The difference between the results of MCNPX and MCNPX-MATS is much smaller than that between MCNPX and MATS. When considering the heat power in the sub-critical blanket and the beam requirement, as listed in table 4, the difference between MCNPX and MATS is about 10% while the difference between MCNPX and MCNPX-MATS is about 1%. These demonstrate that the target simulation dominantly influences the differences observed. It is noteworthy that the neutron fluence and heat density in the sub-critical blanket depend not only on the number of external neutrons but also on their energy. Although the external neutron yield by Geant4 is smaller than that by MATS, Geant4-MATS results in a higher heat density in the sub-critical blanket, leading to a reduced beam requirement.

IV. CONCLUSIONS AND OUTLOOK

Based on the Monte Carlo simulation programs OpenMC and GMT, a program named MATS has been developed, dedicated to the simulation study of the ADS target-reactor system. The physical calculation functions of MATS rely on an electromagnetic interaction

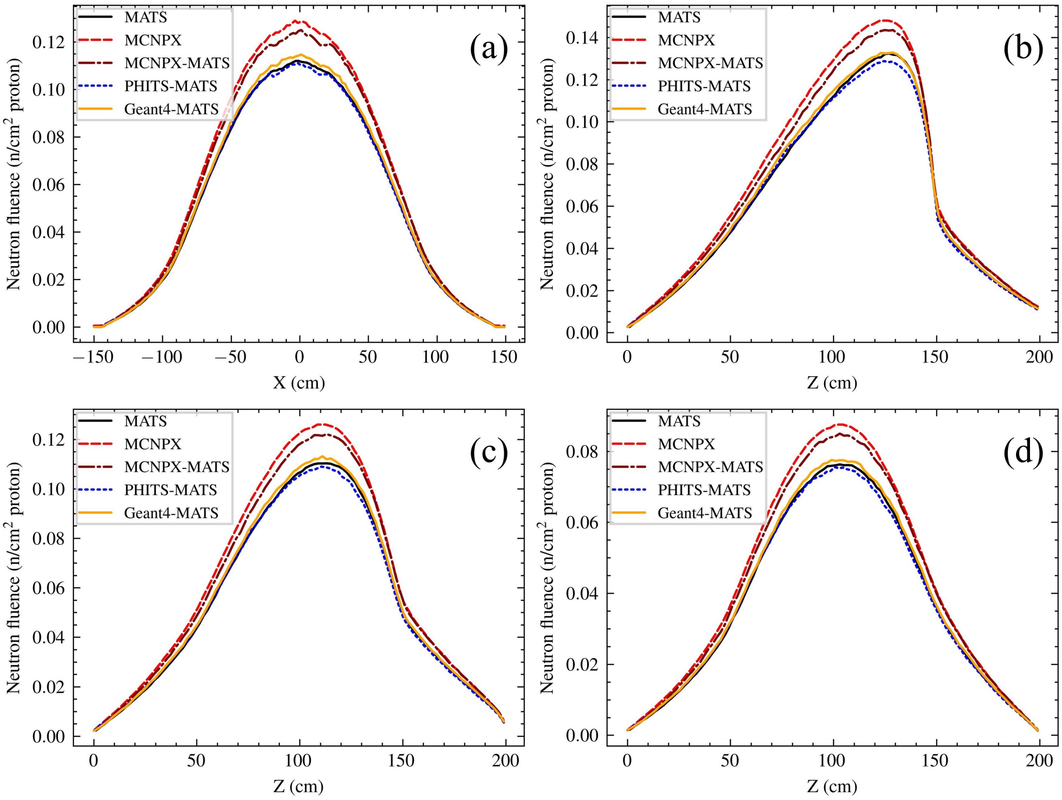

Fig. 13. (Color online) Similar to Fig. 11, but with the addition of MCNPX for the direct simulation. MCNPX, PHITS and Geant4 are used for the first step in the two-step simulations, instead of using MATS.

TABLE 4. Heat released in the sub-critical blanket driven by one proton and the corresponding beam requirements.

Simulation methods	Heat released (GeV/p)	Beam requirements	
		Value (mA)	relative error (%)
MATS	55.9	6.744	/
MATS-MATS	54.6	6.901	2.33
MCNPX	62.6	6.022	-10.7
MCNPX-MATS	61.9	6.090	-9.71
PHITS-MATS	55.1	6.846	1.51
Geant4-MATS	57.1	6.603	-2.10

module, a hadronic interaction module, a high-energy cross-section module, traditional reactor-oriented calculation functions and the nuclear data library. This equips MATS with the capability to simulate the transport processes of particles in a wide-energy range, which is essential for R&D of ADS. This is because the external source efficiency is also sensitive to the neutron energy. It is revealed that there is an underestimation of neutron fluence and heat density, resulting in an overestimation of beam requirement at the level of 10% or more, when the neutrons of energy above 20 MeV are treated as the neutrons of 20 MeV. Besides, the deviations of heat in the sub-critical blanket and beam requirement are at the level of 2%, when protons, gammas, pions and light-nucleus particles from the target are not transported in the sub-critical blanket.

The V&V of the ADS spallation target simulations indicate that MATS provides a medium estimation on neutronics characteristics and heat, compared to MCNPX, PHITS and Geant4. The comparisons reveal that the differences in neutron yield and total heat between MATS and MCNPX are about 8% and 10%, respectively. MATS tends to predict higher heat and lower neutron yield than MCNPX. However, the differences between MATS simulation and those of PHITS and Geant4 are less than 5% for both neutron yield and total heat.

Regarding the target-reactor system, the difference between MCNPX and MATS is like that observed in target simulation. We find that the difference is primarily due to the different predictions in target simulation. Additionally, there are differences in the simulations of high-energy neutrons in sub-critical system. In terms of

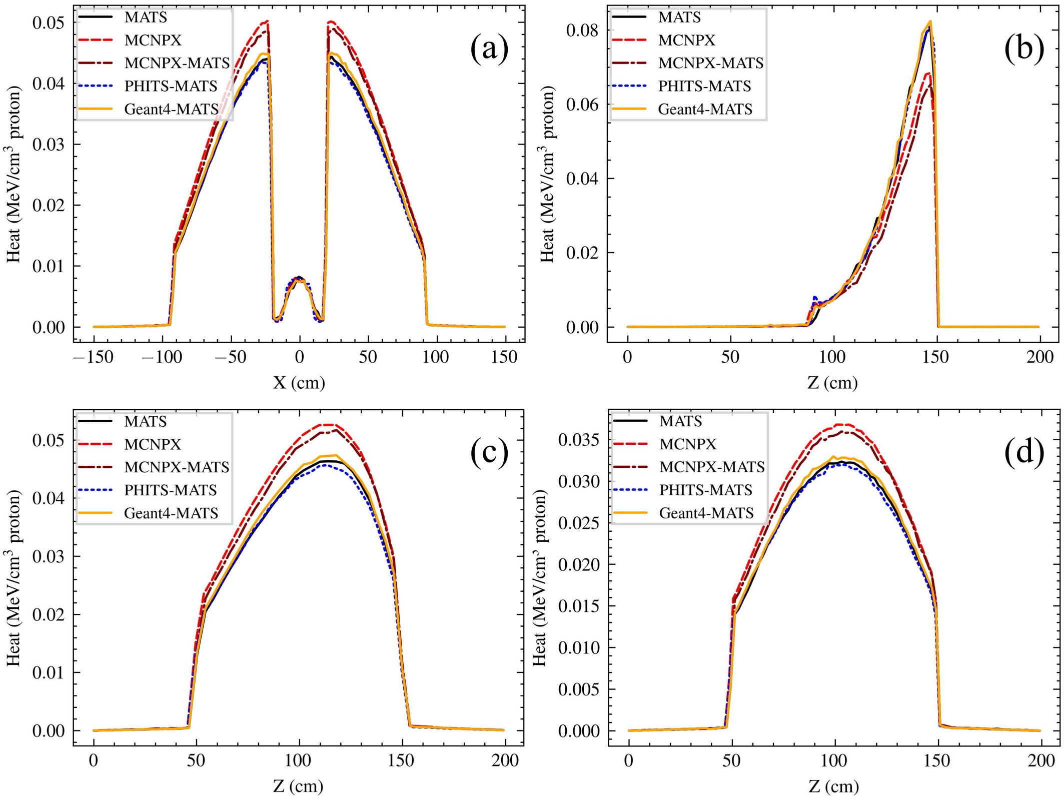

Fig. 14. (Color online) Similar to Fig. 13, but with the data representing heat density.

external source efficiency, the deviation is approximately 4% within the energy range from 100 MeV to 1000 MeV.

To perform an extensive V&V, we employed the two-step method in addition to the direct MCNPX simulation. In these two-step methods, the first-step simulation was performed with different programs, while the second-step simulation was done using MATS. We find that the differences in neutron fluence and heat among Geant4-MATS, PHITS-MATS and MATS-MATS are all smaller than 5%. Our study also demonstrates that the neutron fluence and heat density in the sub-critical blanket depend not only on the number of external neutrons but also on the neutron energy. Compared to benchmark exercise [45] organized by OECD/NEA in 1999, in which the emphasis is on code and data validation in the energy region below 20 MeV, the benchmark presented in this paper is a big step forward. In future, more benchmark exercises based on experimental results may be conducted to clarify the discrepancies.

In summary, the development of the MATS program with the fundamental calculation functions for ADS R&D has been demonstrated to be successful. Further efforts should be made on upgrading reaction modelss [50–52] based on an overall evaluation of the calculations of high-energy neutron-induced reactions on actinide nuclides, and on developing more neutronics calculation functions [53–56] dedicated to the study of subcritical reactors and the R&D of ADS facilities. A user-friendly interface and more widely demanded functions including variance reduction calculations [57], radioactivity and shielding simulation [58, 59] and irradiation dose assessment [60, 61], are also on the to-do list to make MATS a state-of-the-art radiation simulation program for the multidisciplinary applications of accelerator beams [62–64].

V. ACKNOWLEDGMENTS

All authors would like to extend our special thanks to the OpenMC development team, and also to Davide Mancusi for providing us with the source code of the INCL++ model.

[1] C.D. Bowman, E.D. Arthur, P.W. Lisowski et al., Nuclear energy generation and waste transmutation using an accelerator-driven intense thermal neutron source. Nucl. Instrum. Meth. A 320(1–2), 336–367(1992). doi:

10.1016/0168-9002(92)90795-6
[2] L. Mansani, C. Artioli, M. Schikorr et al., The European lead-cooled EFIT Plant: An Industrial-Scale accelerator-driven system for minor actinide transmutation-I. Nucl. Technol. 180(2), 241–263(2012). doi: 10.13182/NT11-96
[3] K. Tsujimoto, T. Sasa, K. Nishihara et al., Neutronics design for lead-bismuth cooled accelerator-driven system for transmutation of minor actinide. J. Nucl. Sci. Technol. 41(1), 21–36(2004). doi: 10.1080/18811248.2004.9715454
[4] X.Z. Li, S.C. Zhou, Y.Q. Zheng et al., Preliminary Studies of a New Accelerator-Driven Minor Actinide Burner in Industrial Scale. Nucl. Eng. Des. 292, 57–68(2015). doi: 10.1016/j.nucengdes.2015.05.019
[5] Y. Gohar, Y. Cao, A.R. Kraus, ADS design concept for disposing of the U.S. spent nuclear fuel inventory. Ann. Nucl. Energy. 160, 108385(2021). doi: 10.1016/j.anucene.2021.108385
[6] H.A. Abderrahim, P. Baeten, D.D. Bruyn et al., MYRRHA - A multi-purpose fast spectrum research reactor, Energy Conversion and Management. 63, 4–10(2012). doi: 10.1016/j.enconman.2012.02.025
[7] L. Gu, X.K. Su, Latest research progress for LBE coolant reactor of China initiative accelerator driven system project. Front. Energy. 15, 810-831(2021). doi: 10.1007/s11708-021-0760-1
[8] Y. He, H. Jia, X.C. Zhang et al., Accelerator driven system—A solution to multiple problems of society. Paper presented at the 14th International Particle Accelerator Conference, Venice, Italy, 7–12 May 2023.https://indico.jacow.org/event/41/contributions/641/
[9] L. Zhang, Y.W. Yang, Y.C. Gao, Preliminary Physics Study of the Lead–Bismuth Eutectic Spallation Target for the China Initiative Accelerator-Driven System. Nucl. Sci. Tech. 27, 120(2016). doi: 10.1007/s41365-016-0114-6
[10] N. Pu, X.C. Zhang, H.J. Cai et al., Evaluation of OpenMC calculations coupling with PHITS, FLUKA, and GEANT4 for ADS study. Prog. Nucl. Energ. 155, 104505(2023). doi: 10.1016/j.pnucene.2022.104505
[11] J. Allison, K. Amako, J. Apostolakis et al., Recent developments in Geant4. Nucl. Instrum. Methods. Phys. Res. Sect. A 835, 186–225(2016). doi: 10.1016/j.nima.2016.06.125
[12] Z.L. Zhao, Y.W. Yang, S. Hong, Application of FLUKA and OpenMC in Coupled Physics Calculation of Target and Subcritical Reactor for ADS. Nucl. Sci. Tech. 30(1), 10(2019). doi: 10.1007/s41365-018-0539-1
[13] Mokhov, V. Nikolai, James et al., The MARS Code System User's Guide Version 15(2016). United States. doi: 10.2172/1462233
[14] T. Sato, K. Niita, N. Matsuda et al., Particle and heavy ion transport code system PHITS, version 2.52. J. Nucl. Sci. Tech. 50, 913–923(2013). doi: 10.1080/00223131.2013.814553
[15] Y. Kadi, The EA-MC code package. Paper presented at the proceedings of an advisory group meeting, Taejon, Republic of Korea, Nov 1–4, 1999. https://1library.net/article/ea-mc-code-package-ea-neutronic-calculations-eap.ydek7x1q
[16] P. Cloth, D. Filges, R.D. Neef et al., HERMES - a Monte Carlo program system for beam-materials interaction studies. Provided by the SAO/NASA Astrophysics Data System, May, 1988.https://ui.adsabs.harvard.edu/abs/1988hmcp.rept.....C
[17] T.A. Gabriel, High Energy Transport Code HETC. Paper presented at the LEP experimenters' workshop on shower simulation, Geneva, Switzerland, 29 Jan 1985. https://www.osti.gov/biblio/6286345
[18] W.A. Coleman, T.W. Armstrong, Nucleon-Meson Transport Code NMTC, ORNL Report 4606, Oak Ridge National Laboratory, Dec 31 1971. doi:10.2172/4096131.
[19] R.E. Preal, H. Lichtenstein, User Guide to LCS: The LAHET Code System, LA-UR-89-3014, Los Alamos National Laboratory, Step 15 1989. https://mcnp.lanl.gov/pdf_files/....pdf
[20] T. Sugawara, K. Nishihara, H. Iwamoto et al., Development of three-dimensional reactor analysis code system for accelerator-driven system, ADS3D and its application with subcriticality adjustment mechanism. J. Nucl. Sci. Tech. 53(12), 2018–2027(2016). doi: 10.1080/00223131.2016.1179600
[21] J.A. Favorite, SENSMG: First-Order Sensitivities of Neutron Reaction Rates, Reaction-Rate Ratios, Leakage, keff, and α Using PARTISN. Nucl. Sci. Tech. 192(1), 80–114(2018). doi: 10.1080/00295639.2018.1471296
[22] J. Chen, Z.Y. Liu, C. Zhao et al., A new high-fidelity neutronics code NECP-X. Ann. Nucl. Energy. 116, 417–428(2018). doi: 10.1016/j.anucene.2018.02.049.
[23] H.C. Wu, L.Z. Cao, Y.Q. Zheng et al., Development and Application of NECP Code Package of Deterministic Nuclear Reactor Physics Code System. Atomic Energy Science and Technology. 53(10), 1833–1841(2019). doi: 10.7538/yzk.2019.53.10.1833
[24] M.Dai, M.S. Cheng, Application of material-mesh algebraic collapsing acceleration technique in method of characteristics-based neutron transport code. Nucl. Sci. Tech. 32(8), 87(2021). doi: 10.1007/s41365-021-00923-w.
[25] M. Dai, A. Zhang, M.S. Cheng, Improvement of the 3D MOC/DD neutron transport method with thin axial meshes. Ann. Nucl. Energy. 185, 109731(2023). doi: 10.1016/j.anucene.2023.109731
[26] D.P. Griesheimer, D.F. Gill, B.R. Nease et al., MC21 v.6.0 – A continuous-energy Monte Carlo particle transport code with integrated reactor feedback capabilities. Ann. Nucl. Energy. 82, 29–40(2015). doi: 10.1016/j.anucene.2014.08.020
[27] J. Leppänen, M. Pusa, T. Viitanen et al., The Serpent Monte Carlo code: status, development and applications in 2013. Ann. Nucl. Energy. 82, 142–150(2015). doi: 10.1016/j.anucene.2014.08.024.
[28] L. Deng, G. Li, B.Y. Zhang et al., A high fidelity general purpose 3-D Monte Carlo particle transport program JMCT3.0. Nucl. Sci. Tech. 33, 108(2022). doi: 10.1007/s41365-022-01092-0
[29] K. Wang, Z.G. Li, D. She et al., RMC – A Monte Carlo code for reactor core analysis. Ann. Nucl. Energy. 82, 121–129(2015). doi: 10.1016/j.anucene.2014.08.048
[30] S.C. Liu, D. She, J.G. Liang et al., Development of random geometry capability in RMC code for stochastic media analysis. Ann. Nucl. Energy. 85, 903–908(2015). doi: 10.1016/j.anucene.2015.07.008
[31] Y.C. Wu, J. Song, H.Q. Zheng et al., CAD-based Monte Carlo program for integrated simulation of nuclear system SuperMC. Ann. Nucl. Energy. 82, 161–168 (2015).

doi: 10.1016/j.anucene.2014.08.058

[32] Q.M. He, Q. Zheng, J. Li et al., NECP-MCX: A hybrid Monte-Carlo-Deterministic particle-transport code for the simulation of deep-penetration problems. Ann. Nucl. Energy. 151, 107978(2021). doi: 10.1016/j.anucene.2020.107978

[33] P.K. Romano, N.E. Horelik, B.R. Herman et al., OpenMC: A state-of-the-art Monte Carlo code for research and development. Ann. Nucl. Energy. 82, 90–97(2015). doi: 10.1016/j.anucene.2014.07.048

[34] G. Mckinney, MCNPX user's manual, Version 2.7.0. LA-CP-11-00438, Los Alamos National Laboratory, Apri 2011. https://www.researchgate.net/.../references

[35] T. Goorley, M. James, T. Booth et al., Initial MCNP6 release overview. Nucl. Technol. 180(3), 298–315(2012). doi: 10.13182/NT11-135

[36] H.J. Cai, F. Fu, J.Y. Li et al., Code Development and Target Station Design for Chinese Accelerator-Driven System Project. Nucl. Sci. Eng. 183(1), 107–115(2016). doi: 10.13182/NSE15-59

[37] H.J. Cai, Z.L. Zhang, F. Fu et al., Toward high-efficiency and detailed Monte Carlo simulation study of the granular flow spallation target. Nucl. Instrum. Meth. A 882, 117–123(2018). doi: 10.1016/j.nima.2017.10.078

[38] P.K. Romano, B. Forget, The OpenMC Monte Carlo Particle Transport Code. Ann. Nucl. Energy. 51, 274–281(2013). doi: 10.1016/j.anucene.2012.06.040

[39] R. J. Glauber, Cross sections in deuterium at high energies. Phys. Rev. 100(1), 242(1955). doi: 10.1103/PhysRev.100.242

[40] S. Goudsmit, J. L. Saunderson, Multiple Scattering of Electrons. Phys. Rev. 57(1), 24(1940). doi: 10.1103/PhysRev.57.24

[41] R. Serber, Nuclear Reactions at High Energies. Phys. Rev. 72(11), 1114(1947). doi: 10.1103/PhysRev.72.1114

[42] H. Zhang, F. Sheng, Y. Fang, Theoretical Methods on Spallation Products of Proton-induced Reactions with Intermediate Energy. Nuclear Physics Review. (04), 239–246(2003). doi: 10.11804/NuclPhysRev.20.04.239

[43] J.-J. Gaimard, K.H. Schmidt, A reexamination of the abrasion-ablation model for the description of the nuclear fragmentation reaction. Nucl. Phys. A 531(3-4), 709-745(1991). doi: 10.1016/0375-9474(91)90748-U

[44] D. Mancusi, R.J. Charity, J. Cugnon, Unified description of fission in fusion and spallation reactions. Phys. Rev. C 82(4), 044610(2010). doi: 10.1103/PhysRevC.82.044610

[45] M. Cometto, B.C. Na, P. Wydler, OECD/Nea benchmark calculations for accelerator driven systems. Paper presented at the information exchange meeting, NEA, Madrid (Spain), 11–13 Dec 2000. https://www.osti.gov/etdeweb/biblio/20246408

[46] S. Leray, D. Mancusi, P. Kaitaniemi et al., Extension of the Liège Intra Nuclear Cascade model to light ion-induced collisions for medical and space applications. J. Phys.: Conf. Ser. 420, 012065 (2013). doi: 10.1088/1742-6596/420/1/012065

[47] A. Boudard, J. Cugnon, J.C. David et al., New potentialities of the Liège intranuclear cascade model for reactions induced by nucleons and light charged particles. Phys. Rev. C 87(1), 014606 (2013). doi: 10.1103/PhysRevC.87.014606

[48] B. Ye, C.W. Yang, C. Zheng, Measurement of k_{eff} by delayed neutron multiplication in subcritical systems. Nucl. Sci. Tech. 29, 29 (2018). doi: 10.1007/s41365-018-0355-7

[49] X.C. Zhang, L. Yu, X.S. Yan et al., The optimization on neutronic performance of the granular spallation target by using low-density porous tungsten. Nucl. Instrum. Meth. A 916, 22–31 (2019). doi: 10.1016/j.nima.2018.08.071

[50] Z. Wei, Z.E. Yao, C.L. Lan et al., Monte Carlo simulation of fission yields, kinetic energy, fission neutron spectrum and decay γ-ray spectrum for 232Th(n,f) reaction induced by 3H(d,n)4He neutron source. J. Radioanal. Nucl. Chem. 305(2),2015(455–462). doi: 10.1007/s10967-014-3910-7

[51] C.L. Lan, M. Peng, Y. Zhang et al., Geant4 simulation of 238U(n,f) reaction induced by D-T neutron source. Nucl. Sci. Tech. 28(1), 8(2017). doi: 10.1007/s41365-016-0158-7

[52] Z. Wei, C.Q. Liu, C. Han et al., Monte-Carlo calculation of fission process for neutron-induced typical actinide nuclei fission. EPJ Web of Conferences. 239, 05015(2020). doi: 10.1051/epjconf/202023905015

[53] Q. Guo, Z.P. Chen, Multi-Regional Delta-Tracking Method for Neutron Transport Tracking in Monte Carlo Criticality Calculation. Sustainability-Basel. 10(7), 2272(2018). doi: 10.3390/su100722727

[54] Z.P. Chen, J.S. Xie, Q. Guo et al., Physics-oriented optimization strategy for the energy lookup algorithm in continuous energy Monte Carlo neutron transport simulation. Comput. Phys. Commum. 234, 146–58(2019). doi: 10.1016/j.cpc.2018.07.016

[55] S.C. Liu, Y. Yuan, J.K. Yu et al., Development of on-the-fly temperature-dependent cross-sections treatment in RMC code. Ann. Nucl. Energy. 94,144–149(2016). doi: 10.1016/j.anucene.2016.02.026

[56] S.C. Liu, X.J. Peng, C. Josey et al., Generation of the windowed multipole resonance data using Vector Fitting technique. Ann. Nucl. Energy. 112, 30–41(2018). doi: 10.1016/j.anucene.2017.09.042

[57] Y.S. Hao, Z. Wu, S.S. Gao, et al., Research on a Monte Carlo global variance reduction method based on an automatic importance sampling method. Nucl. Sci. Tech. 48(5), 86(2024). doi: 10.1007/s41365-024-01404-6

[58] Y. Luo, S. Huang, H. Zhang et al., Assessment of the induced radioactivity in the treatment room of the Heavy Ion Medical Machine in Wuwei using PHITS. Nucl. Sci. Tech. 34(2), 29(2023). doi: 10.1007/s41365-023-01181-8

[59] Z.P. Chen, Z.Y. Zhang, J.S. Xie et al., Multi-objective optimization strategies for radiation shielding design with genetic algorithm. Comput. Phys. Commun. 260, 107267(2021). doi: 10.1016/j.cpc.2020.107267

[60] S.B. TANG, Q.L. Ma, Z.J. Yin et al., Simulation of distribution of radiation energy density in water balls. Nucl. Sci. Tech. 16(6), 347–351(2005). http://www.nst.sinap.ac.cn/article/id/1822?lang=en

[61] X.Y. Luo, R. Qiu, Z. Wu, et al., THUDose$_{PD}$: a three-dimensional Monte Carlo platform for phantom dose assessment. Nucl. Sci. Tech. 34(11), 164(2023). doi: 10.1007/s41365-023-01315-y

[62] W.W. Qiu, W. Sun, J. Su, Neutronic analysis of deuteron-driven spallation target. Nucl. Sci. Tech. 32, 94(2021). doi: 10.1007/s41365-021-00932-9

[63] Z.E. Yao, P. Luo, T. KOBAYASHI et al., Evaluation of D(d,n)3He reaction neutron source models for BNCT irradiation system design. Nucl. Sci. Tech. 18(6), 330–

335(2007). doi: 10.1016/S1001-8042(08)60003-2
[64] D.P. Xu, Z.E. Yao, J.B. Pan et al., Study on the multiple characteristics of M_3 generation of pea mutants obtained by neutron irradiation. Nucl. Sci. Tech. 31(7), 67(2020). doi: 10.1007/s41365-020-00777-8